Radiology: Cardiothoracic Imaging

TECHNICAL DEVELOPMENT

Myocardial Regional Shortening from 4D Cardiac CT Angiography for the Detection of Left Ventricular Segmental Wall Motion Abnormality

Zhennong Chen, PhD • Francisco Contijoch, PhD • Andrew M. Kahn, MD • Seth Kligerman, MD • Hari K. Narayan, MD • Ashish Manohar, PhD • Elliot McVeigh, PhD

From the Departments of Bioengineering (Z.C., F.C., E.M.) and Mechanical and Aerospace Engineering (A.M.), UC San Diego School of Engineering, La Jolla, Calif; and Departments of Radiology (F.C., S.K., E.M.), Cardiology (A.M.K., E.M.), and Pediatrics (H.K.N.), UC San Diego School of Medicine, 9452 Medical Dr, La Jolla, CA 92037. Received June 30, 2022; revision requested August 9; revision received January 22, 2023; accepted January 30. **Address correspondence to** E.M. (email: *emcveigh@ucsd.edu*).

Z.C. and E.M. supported by National Heart, Lung, and Blood Institute grants HL144678 and HL153250. F.C. supported by National Heart, Lung, and Blood Institute grants HL145817 and HL143113. A.M. supported by American Heart Association grant 20PRE35210261.

Conflicts of interest are listed at the end of this article.

Radiology: Cardiothoracic Imaging 2023; 5(2):e220134 • https://doi.org/10.1148/ryct.220134 • Content codes: CA CT

Purpose: To investigate whether endocardial regional shortening computed from four-dimensional (4D) CT angiography (RS_{CT}) can be used as a decision classifier to detect the presence of left ventricular (LV) wall motion abnormalities (WMAs).

Materials and Methods: One hundred electrocardiographically gated cardiac 4D CT studies (mean age, 59 years ± 14 [SD]; 61 male patients) conducted between April 2018 and December 2020 were retrospectively evaluated. Three experts labeled LV wall motion in each of the 16 American Heart Association (AHA) segments as normal or abnormal; they also measured peak RS_{CT} across one heartbeat in each segment. The data set was split evenly into training and validation groups. During training, interchangeability of RS_{CT} thresholding with experts to detect WMA was assessed using the individual equivalence index (γ), and an optimal threshold of the peak RS_{CT} (RS_{CT}*) that achieved maximum agreement was identified. RS_{CT}* was then validated using the validation group, and the effect of AHA segment–specific thresholds was evaluated. Agreement was assessed using κ statistics.

Results: The optimal threshold, RS_{CT}* of -0.19, when applied to all AHA segments, led to high agreement (agreement rate = 92.17%, κ = 0.82) and interchangeability with experts (γ = -2.58%). The same RS_{CT}* also achieved high agreement in the validation group (agreement rate = 90.29%, κ = 0.76, γ = -0.38%). The use of AHA segment–specific thresholds (range: 0.16 to -0.23 across AHA segments) slightly improved agreement (1.79% increase).

Conclusion: RS_{CT} thresholding was interchangeable with expert visual analysis in detecting segmental WMA from 4D CT and may be used as an objective decision classifier.

Supplemental material is available for this article.

Regional myocardial function is important to evaluate in both ischemic and nonischemic heart disease (1–3). Multidetector cardiac CT with electrocardiographically gated dynamic CT scan protocols has enabled assessment of cardiac wall motion by acquiring a series of functional images spanning the full cardiac cycle in just one heartbeat (4,5). Regional left ventricular (LV) wall motion abnormality (WMA) detection using dynamic CT is highly concordant with both echocardiography (6,7) and cardiac MRI (8).

Recently, a surface feature–tracking technique (9) was developed to quantify three-dimensional (3D) endocardial regional shortening from four-dimensional (4D) CT (RS_{CT}) and was validated against tagged cardiac MRI in both animals (10) and humans (11). This technique derives the deformation and displacement of endocardial surface points via nonrigid 3D point set registration (12) to obtain the RS_{CT} of the endocardium. RS_{CT} values have been measured in the normal human LV (5) and in patients before and after transcatheter mitral valve implantation (13). Regional right ventricular systolic dysfunction (14) has also been quantified with RS_{CT}.

The overarching goal of this study was to investigate whether RS_{CT} can be used as a decision classifier to detect the presence of LV WMAs from 4D CT studies. Concretely, we investigated the interchangeability of RS_{CT} with expert visual labeling to detect WMAs and derived an optimal RS_{CT} threshold that achieves maximum agreement with experts.

Materials and Methods

CT Data Collection

This Health Insurance Portability and Accountability Act–compliant study was approved by the institutional review board with a waiver of informed consent. A total of 100 electrocardiographically gated contrast-enhanced cardiac CT angiographic studies between April 2018 and December 2020 were retrospectively collected within a

Abbreviations

AHA = American Heart Association, 4D = four-dimensional, LV = left ventricle, RS_{CT} = regional shortening computed from 4D CT angiography, 3D = three-dimensional, WMA = wall motion abnormality

Summary

Regional endocardial shortening computed from four-dimensional CT angiography demonstrated interchangeability with expert visual labeling in detecting segmental left ventricular wall motion abnormalities.

Key Points

- Endocardial regional shortening computed from four-dimensional CT angiography (RS_{CT}) is an objective, quantitative decision classifier that is interchangeable with expert visual analysis to detect segmental left ventricular wall motion abnormalities.
- An optimal classification threshold of RS_{CT} greater than -0.19 was defined to obtain a high agreement rate with experts in all 16 American Heart Association segments in both a training group (agreement rate = 92.17%, individual equivalence index γ = -2.58%) and a validation group (agreement rate = 90.29%, γ = -0.38%).

Keywords

CT, Left Ventricle, Regional Endocardial Shortening, Wall Motion Abnormality

single institution. Figure 1 shows the patient collection process, and Appendix S1 provides details about inclusion and exclusion criteria. The clinical indications for these 100 studies can be found in Table S1.

All studies were acquired with a single wide-detector CT scanner with 256 detector rows and 16-cm z-axis coverage (Revolution CT; GE Healthcare), allowing for an axial acquisition of the entire heart during a single heartbeat. All studies had functional phases reconstructed at 10% R-R intervals using the vendor default cardiac function image reconstruction method with the standard imaging kernel. The 256 image sections were reconstructed on a 512 × 512-pixel matrix in the axial plane over a field of view of 24 cm ± 2 (SD) with 0.625-mm section thickness. The CT imaging protocol details can be found in Appendix S2.

Visual Labeling of Segmental WMAs

The wall motion classification in each segment was made via visual labeling by three cardiovascular imaging experts (expert a: author A.M.K., >15 years of experience; expert b: author S.K., 14 years of experience; and expert c: author H.K.N., >5 years of experience), who visually inspected the cine movie of cardiac function across a cardiac cycle shown in a set of reformatted cardiac imaging planes (Fig S1) without knowledge of the patient's health record and previous diagnosis. The readers independently scored the wall motion for each segment (segments 1 through 16 in the American Heart Association [AHA] 16-segment model) by visual inspection. The scores were given as follows: 0 for normal motion, 1 for hypokinetic, 2 for akinetic, and 3 for dyskinetic. Scores 1–3 were further grouped as abnormal wall motion.

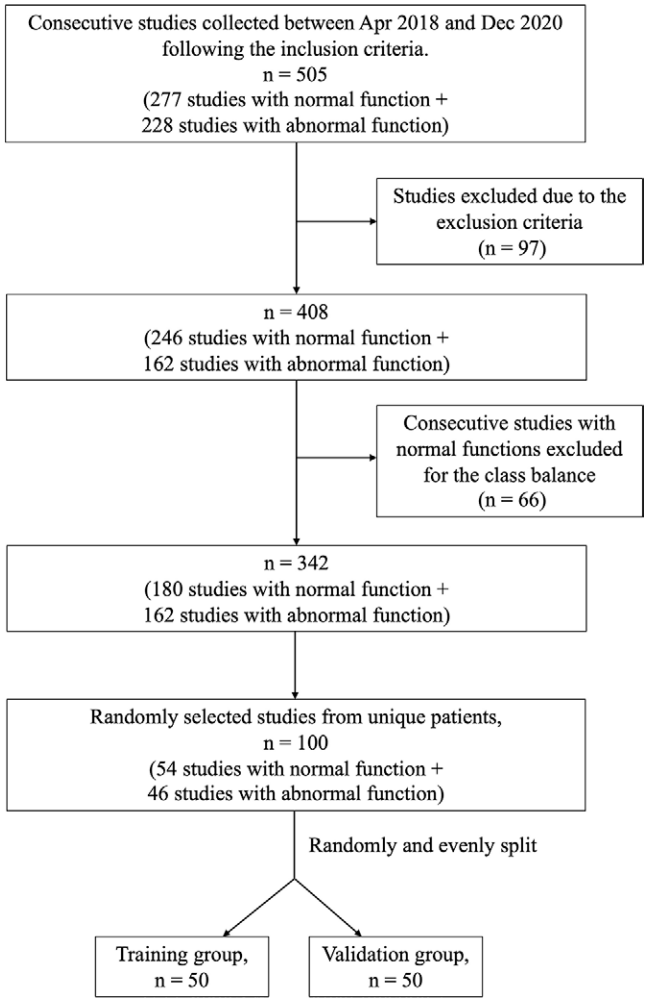

Figure 1: Flowchart of CT study selection for analysis. Note that both normal and abnormal function in the flowchart refer to the imaging reports, which were only used for prescreening. Inclusion and exclusion criteria are listed in Appendix S1.

Quantitative Image Analysis

The voxelwise LV blood-pool segmentation was created by a pretrained deep learning segmentation U-Net (15) and then manually refined in ITK-SNAP software, version 3.4.0 *(www.itksnap.org)* (16). Second, the CT image volume was rotated to align the LV long axis with the z-axis of the image. After LV volume segmentation, a temporal sequence of the binary LV volumes across the entire cardiac cycle was sent to the RS_{CT} pipeline (9) for automatic quantitative analysis. Triangular meshes of the endocardial surface were extracted. Then, a 3D nonrigid point set registration (12) was performed to register the endocardial mesh at the reference time frame (defined here as end diastole) to the meshes created for other time frames. Regional shortening (RS_{CT}) at a time frame t was calculated at each triangular face on the endocardial mesh as:

$$RS_{CT} = \sqrt{\frac{Area_t}{Area_{ED}}} - 1 \quad (1),$$

where $Area_t$ is the area of an endocardial mesh face at time frame t and $Area_{ED}$ is the area of the same mesh face at end

diastole. RS_{CT} quantifies the shortening of an endocardial patch at two time frames, and smaller RS_{CT} (more negative) indicates more shortening; for example, RS_{CT} of -0.2 indicates 20% shortening. RS_{CT} for an endocardial surface voxel was calculated as the mean RS_{CT} value of a patch of mesh faces directly connected with each voxel.

We computed a segmental RS_{CT} as the mean RS_{CT} for all the voxels from each AHA segment. We defined a segmental "peak RS_{CT}" as the maximum absolute value of segmental RS_{CT} across all time frames. Note that peak RS_{CT} is not always the RS_{CT} at end systole; a comparison of peak RS_{CT} and end-systolic RS_{CT} can be found in Figure S2. Further details of the above workflow (LV segmentation and RS_{CT} analysis) with comprehensive figures can be found in Colvert et al (13).

Interchangeability Analysis and Definition of Optimal Threshold of RS_{CT}

RS_{CT} thresholding.— A segment was defined as abnormal or normal by the selected threshold value of the peak RS_{CT}:

$$\text{segmental motion} = \begin{cases} \text{abnormal, if its peak } RS_{CT} \geq \text{threshold} \\ \text{normal, if its peak } RS_{CT} < \text{threshold} \end{cases} \quad (2).$$

Given that RS_{CT} always had a negative value, an RS_{CT} value larger than a threshold indicated a smaller strain.

Interchangeability analysis.— We investigated the interchangeability of RS_{CT} thresholding with expert visual labeling using the individual equivalence index denoted as γ (17,18). Specifically, we evaluated interchangeability by comparing *(a)* the *intramethod interreader agreement rate* when all expert readers made the visual labeling with *(b)* the *intermethod agreement rate* when RS_{CT} thresholding was compared with each independent expert. Mathematically, we defined Y_{iRj} to denote the result of visual labeling by reader *j* (*j* = a, b, and c for three readers) on segment *i* and defined Y_{iT} to denote the result of RS_{CT} on segment *i*. Following the idea in Obuchowski et al (17), we defined the individual equivalence index γ as follows:

$$\gamma = \frac{\sum_{i=1}^{N}\sum_{j=a,j'=b;j=a,j'=c;j=b,j'=c}\pi_{R,R}}{3N} - \frac{\sum_{i=1}^{N}\sum_{j=a,b,c}\pi_{T,R}}{3N} \quad (3),$$

where the $\pi_{R,R}$ evaluates the intramethod interreader agreement: It equals 1 when the detection of WMA made by two experts is the same (ie, $Y_{iRj} = Y_{iRj'}$) and equals 0 otherwise; $\pi_{T,R}$ evaluates the intermethod agreement, and it equals 1 when the RS_{CT} has the same result as the experts (ie, $Y_{iRj} = Y_{iT}$, *j* = a, b, or c for three readers) and equals 0 otherwise. *N* denotes the total number of segments. The 95% CI of γ was calculated using bootstrapping methods (18). The interchangeability of two methods was defined as γ of less than +5% limit (18). Figure S3 provides an illustration of how γ is calculated.

Data split and optimal threshold of RS_{CT}.— We randomly and evenly split the data set (*n* = 100) into a training group (*n* = 50) and a validation group (*n* = 50). Therefore, each group had 800 segments (16 segments per study).

The first item in Equation 3 (the interreader agreement rate) had a fixed value in our study, while the second item (the intermethod agreement rate) was dependent on the selected threshold values of RS_{CT} to call a segment abnormal (Eq 2). Therefore, using the training group, we first analyzed the relationship between γ and RS_{CT} threshold values and then defined an optimal threshold of RS_{CT}, denoted as RS_{CT}*, to be the threshold that led to the minimum value of γ (equivalently, RS_{CT}* led to the maximum intermethod agreement rate). Here, RS_{CT}* was a single threshold that we proposed to apply to all 16 AHA segments. We then validated the agreement rate of the RS_{CT}* in the independent validation group.

AHA segment–specific optimal thresholds.— Given the heterogeneity of endocardial wall motion (19) among the AHA segments, we performed an exploratory analysis to define AHA segment–specific optimal thresholds (notation: $RS_{CT,AHA}$*) that maximized the agreement rate with experts in each of the 16 AHA segments. To maximize the amount of data for each AHA segment, we used the entire data set (in total, 100 studies) for each one. We compared the γ by RS_{CT} and by $RS_{CT,AHA}$* in the validation group to evaluate whether using $RS_{CT,AHA}$* improved the performance.

Statistical Analysis

To further assess agreement, we performed κ analysis. We calculated the interreader agreement of classifying a segmental wall motion into normal or abnormal among the three experts using a Conger κ (20). We also calculated the interreader agreement of further classifying abnormal segments into hypokinetic, akinetic, and dyskinetic. For intermethod agreement, we used Cohen κ to compare RS_{CT} results with each of three experts. To avoid the potential dependency among the AHA segments, the κ analyses were performed for each AHA segment individually. The statistical analyses were performed by Python version 3.8 *(https://www.python.org/)* with SciPy version 1.5.2 *(https://scipy.org/)*. Statistical significance was set at a $P \leq .05$. κ value interpretation followed the guideline in Landis and Koch (21).

Results

Data Set Characteristics

The data set characteristics are shown in Table 1. The expert score list is shown in Tables S2 and S3.

Performance of RS_{CT} in Detection of WMA

Histograms of peak RS_{CT} in the training and validation groups.— Figure 2 shows the histogram of peak RS_{CT} for both groups. We observed that all RS_{CT} intervals had one class dominating at least 80% of the data within the 0.05 bin width, except the interval from -0.20 to -0.15, where the two classes were nearly evenly distributed (normal:abnormal = 37:27 in training and 44:33 in validation). No significant structure was observed in the histogram when bin width was reduced.

Table 1: Patient Characteristics

Characteristic	Entire Data Set	Training Group	Validation Group	*P* Value
Data set size	100	50	50	
Age (y)*	59 ± 14	59 ± 15	59 ± 13	
Male (%)†	61	58	64	.54
LVEF				
Median (%)†	62.4	62.1	63.8	
< 40%	22	12	10	
41%–49%	11	4	7	
≥ 50%	67	34	33	
No. of abnormal segments	432 (of 1600, 27%)	219 (of 800, 27%)	213 (of 800, 27%)	.73
Globally normal studies	54	28	26	.69
Globally abnormal studies	12	7	5	.54
Regionally abnormal studies	34	15	19	.40

Note.—Unless otherwise indicated, data are numbers of CT studies. *P* value less than .05 is significant. LVEF = left ventricular ejection fraction.
* Data are means ± SDs.
† Data are percentages.

Interchangeability analysis for RS_{CT}, definition of optimal RS_{CT} threshold.— Figure 3 shows the relationship between the individual equivalence index, γ, and the RS_{CT} threshold values. From the plot, we defined the optimal threshold as RS_{CT}* equals -0.19, which minimized γ, indicating maximization of the intermethod agreement rate. Table 2 shows that in the training group, the interreader agreement rate among the three experts was 2150 of 2400 (89.58%), while RS_{CT}* of -0.19 led to an intermethod agreement rate of 2212 of 2400 (92.17%) and γ of -2.58% (95% CI: -2.61%, -2.57%). This γ did not exceed the +5% limit, indicating interchangeability between experts and RS_{CT}*. Furthermore, this value shows that by switching between the experts and RS_{CT}*, agreement can increase by 2.58% compared with switching among different experts.

We also demonstrated high agreement rates of RS_{CT}* for each of the 16 AHA segments (Table 2), showing γ ranges from -6.00% to 3.33%, with a median value of -2.67% (IQR: -4.00% to -1.83%) across all AHA segments.

RS_{CT}* performance on the validation group.— The same RS_{CT}* was applied to all 800 segments in the validation group and demonstrated high agreement with experts, as well. The interreader agreement rate was 2158 of 2400 (89.92%), while RS_{CT}* led to an intermethod agreement rate of 2167 of 2400 (90.29%) and γ of -0.38% (95% CI: -0.40%, -0.35%) (Table 2). This γ indicates the interchangeability between experts and RS_{CT}*. Further, γ ranged from -6.00% to 4.67%, with median value of -0.67% (IQR: -3.00% to 3.50%) across all AHA segments. The performance of RS_{CT}* across different clinical indications can be found in Table S6.

κ *analysis.—* Interreader agreement analysis among our three experts indicated a median Conger κ score of 0.75 across all AHA segments in classifying segmental wall motion into normal versus abnormal, indicating strong agreement. The Conger κ dropped to a median of 0.39 in subclassifying an abnormal segment into hypokinetic, akinetic, and dyskinetic categories, which reflects fair agreement.

Regarding intermethod agreement, κ values between RS_{CT} and individual experts a, b, and c had a median of 0.85, 0.75, and 0.87, respectively, across all AHA segments in the training group and 0.82, 0.69, and 0.76, respectively, in the validation group; all values indicate strong agreement. The detailed results of all κ analyses can be found in Table S4.

Exploratory Analysis of AHA Segment–specific Optimal $RS_{CT,AHA}$*

In this analysis, we sought to define different thresholds for each specific AHA segment ($RS_{CT,AHA}$*). Figure 4 illustrates that $RS_{CT,AHA}$* ranged from -0.16 to -0.23 across the AHA segments. By switching from the single-threshold RS_{CT}* to the AHA-specific threshold $RS_{CT,AHA}$* in the validation group, we further decreased γ from -0.38% to -2.17% for all segments, corresponding to a 1.79% increase in the agreement between RS_{CT} and experts. Detailed results are reported in Table S5.

Discussion

Our study demonstrated that regional endocardial shortening computed from 4D CT angiography (RS_{CT}) is an objective, quantitative decision classifier that is interchangeable with expert visual analysis to detect segmental LV wall motion abnormalities. An optimal classification threshold of RS_{CT} greater than -0.19 was defined to obtain a high agreement rate with experts in all 16 AHA segments in both a training group (intermethod agreement rate = 92.17%, γ = -2.58%) and a validation group (intermethod agreement

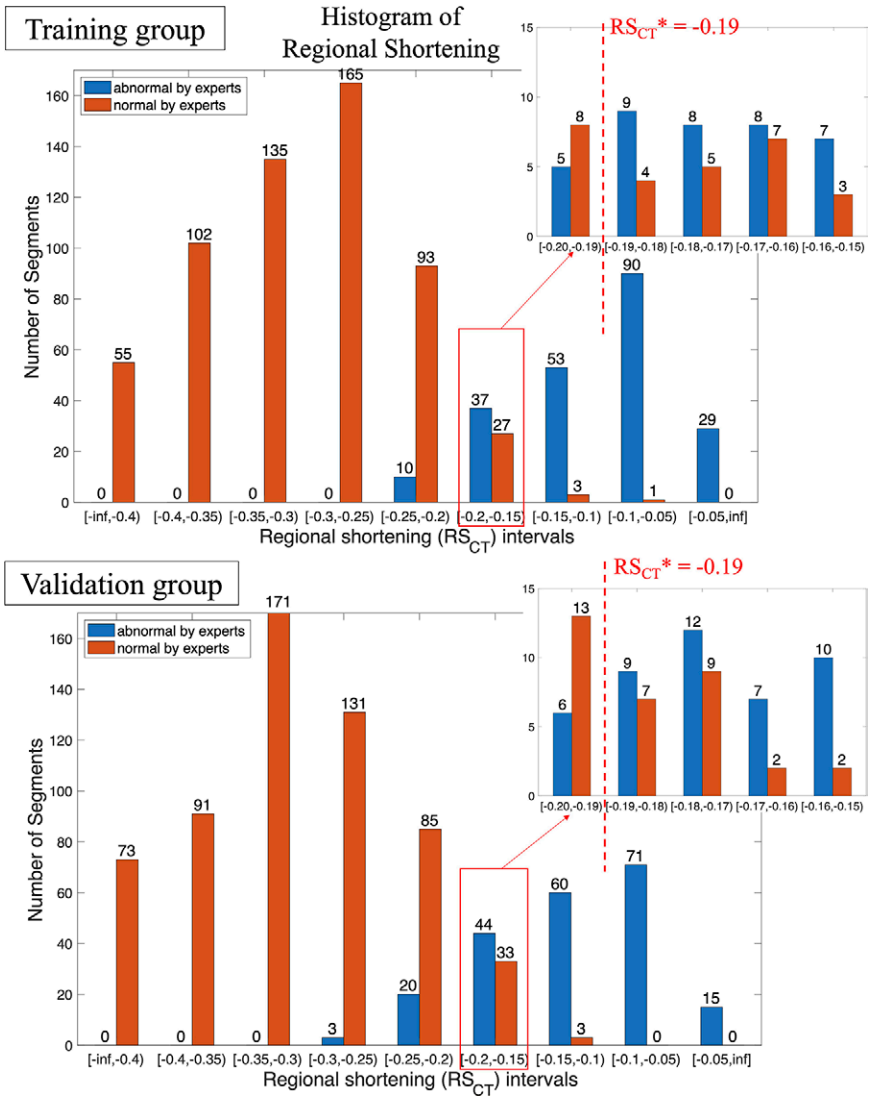

Figure 2: Histogram of the number of segments for peak RS_{CT} intervals in (top) training and (bottom) validation groups. A zoomed-in histogram was made for the RS_{CT} interval with the highest overlap in class (-0.20 to -0.15). The optimal threshold RS_{CT}* was -0.19. RS_{CT} = regional shortening from CT.

rate = 90.29%, γ = -0.38%). We also performed an exploratory analysis to define AHA segment–specific RS_{CT} thresholds; $RS_{CT,AHA}$* values ranged from -0.16 to -0.23, suggesting that the uniform RS_{CT}* equals -0.19 chosen in our main study is broadly appropriate.

There are two main categories of techniques to detect LV WMAs from 4D CT via quantifying the regional myocardial deformation. One category uses image registration to track the motion of small myocardium patches (7), while the other uses a deformable LV model that accounts for the elasticity and incompressibility of the myocardium (6,22). Furthermore, Chen et al (23) recently proposed a deep learning–based method that leverages direct observation of the volume rendering of 4D CT for WMA detection. The method using RS_{CT} evaluated in this article differs from those mentioned above; our proposed method (9,13,24) provides objective quantification of endocardial regional shortening by tracking the motion of endocardial meshes via 3D point registration. Our technique has three main advantages. First, it is not limited on 2D imaging planes, which can be confounded by through-plane motion and foreshortening artifacts (25), but rather it derives 3D measurements from the full 4D CT data. Second, our technique requires no subjective contouring of myocardial boundaries, making the method extremely objective and reproducible. Third, the data are acquired in a single heartbeat, without the need for an expert imaging technician.

Our study had limitations. First, we defined a threshold to separate normal wall motion from all three categories of hypokinetic wall motion by combining expert scores 1–3 (hypokinetic, akinetic, and dyskinetic) into one "abnormal" class. This was done for two reasons: *(a)* The small number of akinetic and dyskinetic segments would lead to severe class imbalance (see Tables S2 and S3), and *(b)* the interobserver agreement in classifying an abnormal motion as hypokinetic, akinetic, or dyskinetic was poor (κ = 0.39). Future work is

underway to evaluate appropriate thresholds for classifying LV wall motion into all four classes. Second, the training and validation groups were derived from the same center and shared similar characteristics (all *P* values > .05 in Table 1).

We demonstrated that regional endocardial shortening from 4D CT (RS_{CT}) was interchangeable with expert visual analysis in detecting segmental WMAs from 4D CT and may be used as an objective decision classifier. Further validation of our method on an independent, large data set from other centers is required to investigate generalizability.

Acknowledgment: The authors thank Gabrielle Colvert, PhD, for her efforts in establishing the initial analysis pipeline for RS_{CT} from 4D CT.

Author contributions: Guarantors of integrity of entire study, **Z.C., E.M.**; study concepts/study design or data acquisition or data analysis/interpretation, all authors; manuscript drafting or manuscript revision for important intellectual content, all authors; approval of final version of submitted manuscript, all authors; agrees to ensure any questions related to the work are appropriately resolved, all authors; literature research, **Z.C., E.M.**; clinical studies, **Z.C., A.M.K., S.K., H.K.N., E.M.**; experimental studies, **Z.C., F.C., A.M., E.M.**; statistical analysis**, Z.C., S.K., E.M.**; and manuscript editing, all authors

Disclosures of conflicts of interest: **Z.C.** National Heart, Lung, and Blood Institute. **F.C.** Research support from GE Healthcare unrelated to this work. **A.M.K.** No relevant relationships. **S.K.** Deputy editor of *Radiology: Cardiothoracic Imaging*. **H.K.N.** No relevant relationships. **A.M.** American Heart Association predoctoral fellowship. **E.M.** National Institutes of Health grants; founder shares in Clearpoint Neuro Inc.

References

1. Flachskampf FA, Schmid M, Rost C, Achenbach S, DeMaria AN, Daniel WG. Cardiac imaging after myocardial infarction. Eur Heart J 2011;32(3):272–283.
2. Jurado-Román A, Agudo-Quílez P, Rubio-Alonso B, et al. Superiority of wall motion score index over left ventricle ejection fraction in predicting cardiovascular events after an acute myocardial infarction. Eur Heart J Acute Cardiovasc Care 2019;8(1):78–85.
3. Yan RT, Bluemke D, Gomes A, et al. Regional left ventricular myocardial dysfunction as a predictor of incident cardiovascular events MESA (multi-ethnic study of atherosclerosis). J Am Coll Cardiol 2011;57(17):1735–1744.

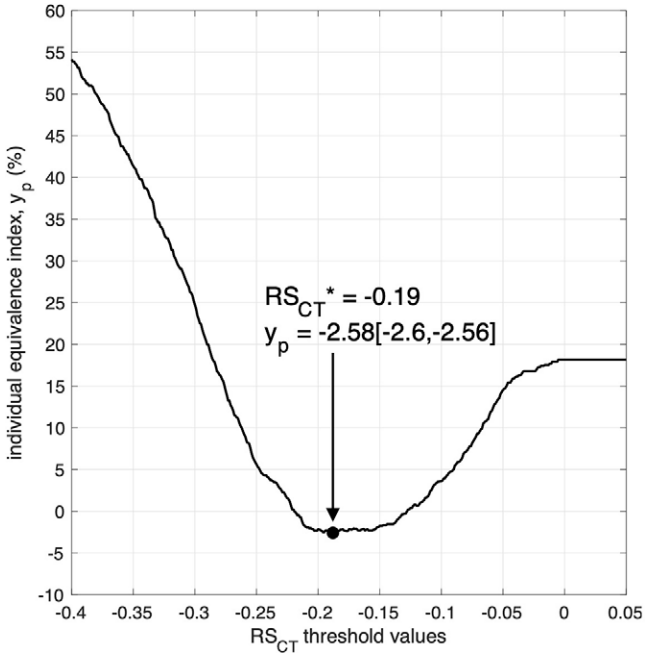

Figure 3: Plot shows relationship between individual equivalence index γ and RS_{CT} threshold values. The optimal threshold RS_{CT}* (black dot) was -0.19, leading to γ of -2.58% (95% CI: -2.61%, -2.57%). RS_{CT} = regional shortening from CT.

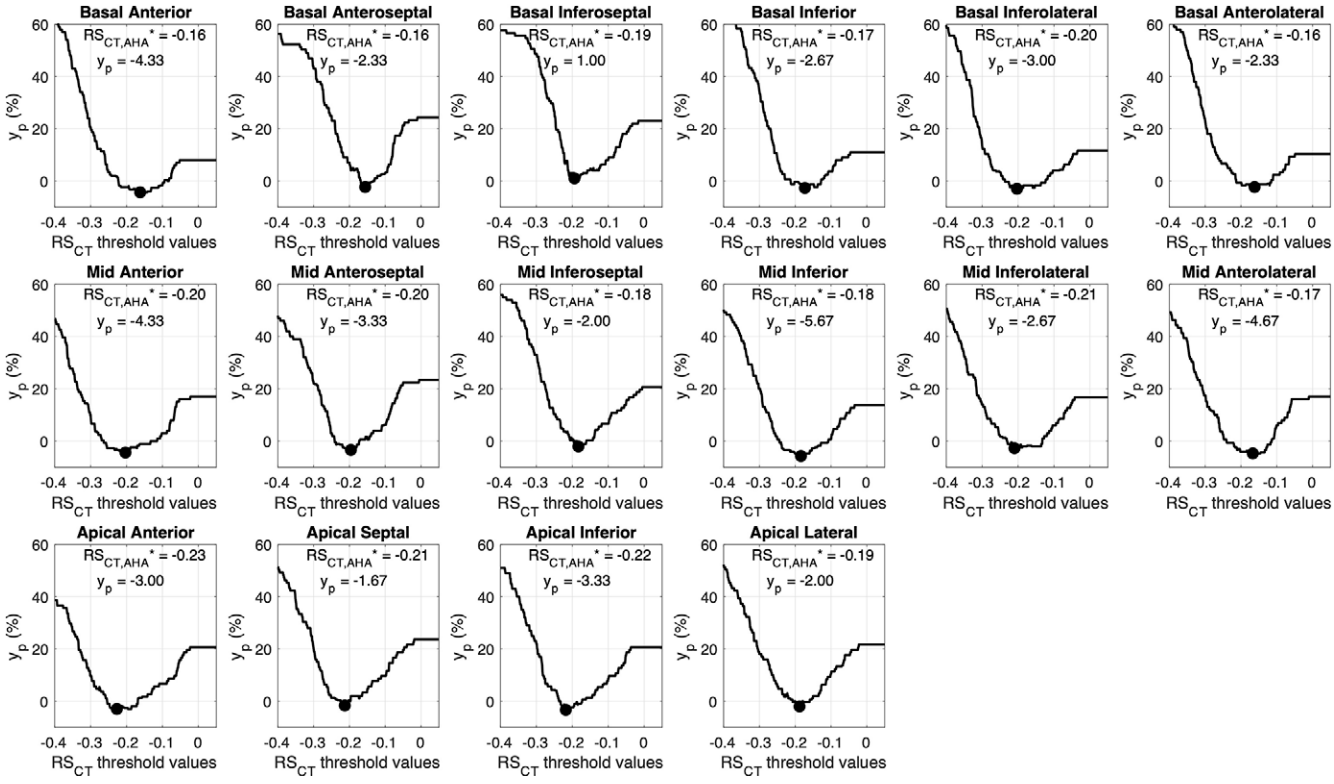

Figure 4: Plots show relationship between individual equivalence index γ and RS_{CT} threshold values for each AHA segment. The entire data set (100 studies) was used. Black dots represent the AHA segment–specific optimal threshold, $RS_{CT,AHA}$*. AHA = American Heart Association, RS_{CT} = regional shortening from CT.

Table 2: Intramethod Interreader Agreement Rate, Intermethod Agreement Rate, Individual Equivalence Index (γ) and Its 95% CI Using RS_{CT}* of -0.19

Parameter	Intramethod Interreader Agreement Rate	Intermethod Agreement Rate	Individual Equivalence Index, γ (%)	95% CI
Training group				
All segments	2150/2400 (89.58)	2212/2400 (92.17)	−2.58	-2.61, -2.57
Basal				
Anterior	134/150 (89.3)	138/150 (92.0)	−2.67	-2.72, -2.60
Anteroseptal	136/150 (90.7)	131/150 (87.3)	3.33	3.23, 3.46
Inferoseptal	138/150 (92.0)	141/150 (94.0)	−2.00	-2.05, -1.98
Inferior	136/150 (90.7)	140/150 (93.3)	−2.67	-2.78, -2.61
Inferolateral	138/150 (92.0)	140/150 (93.3)	−1.33	-1.40, -1.25
Anterolateral	138/150 (92.0)	140/150 (93.3)	−1.33	-1.40, -1.25
Mid				
Anterior	132/150 (88.0)	141/150 (94.0)	−6.00	-6.08, -5.96
Anteroseptal	132/150 (88.0)	138/150 (92.0)	−4.00	-4.07, -3.90
Inferoseptal	136/150 (90.7)	141/150 (94.0)	−3.33	-3.35, -3.26
Inferior	132/150 (88.0)	136/150 (90.7)	−2.67	-2.73, -2.56
Inferolateral	130/150 (86.7)	136/150 (90.7)	−4.00	-4.10, -3.92
Anterolateral	134/150 (89.3)	137/150 (91.3)	−2.00	-2.02, -1.95
Apical				
Anterior	132/150 (88.0)	140/150 (93.3)	−5.33	-5.41, -5.31
Septal	136/150 (90.7)	136/150 (90.7)	0.00	-0.07, 0.14
Inferior	128/150 (85.3)	135/150 (90.0)	−4.67	-4.72, -4.54
Lateral	138/150 (92.0)	142/150 (94.7)	−2.67	-2.70, -2.62
Validation group				
All segments	2158/2400 (89.92)	2167/2400 (90.29)	−0.38	-0.40, -0.35
Basal				
Anterior	130/150 (86.7)	136/150 (90.7)	−4.00	-4.10, -3.92
Anteroseptal	138/150 (92.0)	131/150 (87.3)	4.67	4.65, 4.94
Inferoseptal	136/150 (90.7)	130/150 (86.7)	4.00	3.89, 4.16
Inferior	136/150 (90.7)	135/150 (90.0)	0.67	0.58, 0.77
Inferolateral	134/150 (89.3)	140/150 (93.3)	−4.00	-4.08, -3.98
Anterolateral	134/150 (89.3)	137/150 (91.3)	−2.00	-2.02, -1.95
Mid				
Anterior	136/150 (90.7)	134/150 (89.3)	1.33	1.28, 1.48
Anteroseptal	134/150 (89.3)	138/150 (92.0)	−2.67	-2.77, -2.59
Inferoseptal	138/150 (92.0)	133/150 (88.7)	3.33	3.26, 3.49
Inferior	126/150 (84.0)	136/150 (90.7)	−6.67	-6.82, -6.71
Inferolateral	136/150 (90.7)	137/150 (91.3)	−0.67	-0.73, -0.53
Anterolateral	132/150 (88.0)	141/150 (94.0)	−6.00	-6.02, -5.91
Apical				
Anterior	136/150 (90.7)	137/150 (91.3)	−0.67	-0.80, -0.60
Septal	134/150 (89.3)	128/150 (85.3)	4.00	3.90, 4.16
Inferior	140/150 (93.3)	134/150 (89.3)	4.00	3.93, 4.16
Lateral	138/150 (92.0)	140/150 (93.3)	−1.33	-1.42, -1.26

Note.—Unless otherwise indicated, data are numbers, with percentages in parentheses. Intramethod interreader agreement rate (the third column) shows the agreement between every two experts of the total three experts. There are 800 segments in each group. According to Equation 3, we had 3*N* comparison, so that the denominator of the agreement rate for "All segments" is 800 × 3 = 2400. For each American Heart Association (AHA) segment, 50 in each group; thus, the denominator of the agreement rate is 50 × 3 = 150. Intermethod agreement rate (the fourth column) shows the agreement between RS_{CT}* and each of the three readers; therefore, we also had 3*N* comparison and denominator of the agreement rate as 2400 and 150, respectively. Individual equivalence index, γ, is equal to the value in the third column minus the value in the fourth column. RS_{CT} = regional shortening from CT, RS_{CT}* = the optimal threshold of RS_{CT} that led to the minimum value of γ.

4. Taylor AJ, Cerqueira M, Hodgson JM, et al. ACCF/SCCT/ACR/AHA/ASE/ASNC/NASCI/SCAI/SCMR 2010 Appropriate Use Criteria for Cardiac Computed Tomography. A report of the American College of Cardiology Foundation Appropriate Use Criteria Task Force, the Society of Cardiovascular Computed Tomography, the American College of Radiology, the American Heart Association, the American Society of Echocardiography, the American Society of Nuclear Cardiology, the North American Society for Cardiovascular Imaging, the Society for Cardiovascular Angiography and Interventions, and the Society for Cardiovascular Magnetic Resonance. Circulation 2010;122(21):e525–e555.
5. McVeigh ER, Pourmorteza A, Guttman M, et al. Regional myocardial strain measurements from 4DCT in patients with normal LV function. J Cardiovasc Comput Tomogr 2018;12(5):372–378.
6. Lamash Y, Fischer A, Carasso S, Lessick J. Strain analysis from 4-D cardiac CT image data. IEEE Trans Biomed Eng 2015;62(2):511–521.
7. Buss SJ, Schulz F, Mereles D, et al. Quantitative analysis of left ventricular strain using cardiac computed tomography. Eur J Radiol 2014;83(3):e123–e130.
8. Kaniewska M, Schuetz GM, Willun S, Schlattmann P, Dewey M. Noninvasive evaluation of global and regional left ventricular function using computed tomography and magnetic resonance imaging: a meta-analysis. Eur Radiol 2017;27(4):1640–1659.
9. Pourmorteza A, Schuleri KH, Herzka DA, Lardo AC, McVeigh ER. A new method for cardiac computed tomography regional function assessment: stretch quantifier for endocardial engraved zones (SQUEEZ). Circ Cardiovasc Imaging 2012;5(2):243–250.
10. Pourmorteza A, Chen MY, van der Pals J, Arai AE, McVeigh ER. Correlation of CT-based regional cardiac function (SQUEEZ) with myocardial strain calculated from tagged MRI: an experimental study. Int J Cardiovasc Imaging 2016;32(5):817–823.
11. Manohar A, Colvert GM, Ortuño JE, et al. Regional left ventricular endocardial strains estimated from low-dose 4DCT: comparison with cardiac magnetic resonance feature tracking. Med Phys 2022;49(9):5841–5854.
12. Myronenko A, Song X. Point set registration: coherent point drift. IEEE Trans Pattern Anal Mach Intell 2010;32(12):2262–2275.
13. Colvert GM, Manohar A, Contijoch FJ, et al. Novel 4DCT method to measure regional left ventricular endocardial shortening before and after transcatheter mitral valve implantation. Struct Heart 2021;5(4):410–419.
14. Contijoch FJ, Groves DW, Chen Z, Chen MY, McVeigh ER. A novel method for evaluating regional RV function in the adult congenital heart with low-dose CT and SQUEEZ processing. Int J Cardiol 2017;249:461–466.
15. Chen Z, Rigolli M, Vigneault DM, et al. Automated cardiac volume assessment and cardiac long- and short-axis imaging plane prediction from electrocardiogram-gated computed tomography volumes enabled by deep learning. Eur Heart J Digit Health 2021;2(2):311–322.
16. Yushkevich PA, Piven J, Hazlett HC, et al. User-guided 3D active contour segmentation of anatomical structures: significantly improved efficiency and reliability. Neuroimage 2006;31(3):1116–1128.
17. Obuchowski NA, Subhas N, Schoenhagen P. Testing for interchangeability of imaging tests. Acad Radiol 2014;21(11):1483–1489.
18. Zanchi F, Richard R, Hussami M, Monier A, Knebel JF, Omoumi P. MRI of non-specific low back pain and/or lumbar radiculopathy: do we need T1 when using a sagittal T2-weighted Dixon sequence? Eur Radiol 2020;30(5):2583–2593.
19. Augustine D, Lewandowski AJ, Lazdam M, et al. Global and regional left ventricular myocardial deformation measures by magnetic resonance feature tracking in healthy volunteers: comparison with tagging and relevance of gender. J Cardiovasc Magn Reson 2013;15(1):8.
20. Gwet KL. Testing the difference of correlated agreement coefficients for statistical significance. Educ Psychol Meas 2016;76(4):609–637.
21. Landis JR, Koch GG. The measurement of observer agreement for categorical data. Biometrics 1977;33(1):159–174.
22. Peled Z, Lamash Y, Carasso S, et al. Automated 4-dimensional regional myocardial strain evaluation using cardiac computed tomography. Int J Cardiovasc Imaging 2020;36(1):149–159.
23. Chen Z, Contijoch F, Colvert GM, et al. Detection of left ventricular wall motion abnormalities from volume rendering of 4DCT cardiac angiograms using deep learning. Front Cardiovasc Med 2022;9:919751.
24. Manohar A, Colvert GM, Schluchter A, Contijoch F, McVeigh ER. Anthropomorphic left ventricular mesh phantom: a framework to investigate the accuracy of SQUEEZ using Coherent Point Drift for the detection of regional wall motion abnormalities. J Med Imaging (Bellingham) 2019;6(4):045001.
25. Ünlü S, Duchenne J, Mirea O, et al. Impact of apical foreshortening on deformation measurements: a report from the EACVI-ASE Strain Standardization Task Force. Eur Heart J Cardiovasc Imaging 2020;21(3):337–343.

10.1148/ryct.220134

Appendix S1. Patient Selection

Initially, we retrospectively collected 505 consecutive ECG-gated contrast-enhanced cardiac CT angiography studies conducted between April 2018 and December 2020 within a single institution, given the following inclusion criteria: (1) studies with full *R*-wave to *R*-wave (RR) coverage and (2) studies with an imaging report including the explicit demonstration of cardiac function as normal or abnormal. Note that the imaging reports were used *only* to prescreen the studies to maintain class balance between patients with normal function and those with abnormal function in the study dataset. Subsequently, ninety-seven studies were excluded due to presence of pacing lead artifacts in the left ventricular (LV) chamber, limited field-of-view failing to capture the entire LV, and inadequate image quality; then, 66 consecutive studies from August 2020 to December 2020 were excluded to maintain class balance (Fig 1). Due to the extensive labor required to manually score the per-segment wall motion in a large dataset, we further reduced our study sample by randomly selecting 100 studies from the remaining 342 studies while ensuring these 100 studies were from unique patients. The random selection ensured no introduction of bias in the selection process.

Appendix S2. CT Protocol Details

All studies were acquired by a single wide-detector CT scanner with 256 detector rows and 16 cm z-axis coverage (Revolution CT scanner; GE Healthcare), allowing for a single axial acquisition of the entire heart during a single heartbeat. The iodinated contrast agent iohexol (Omnipaque 350; GE Healthcare) was injected at 4–6 mL per sec for 12 sec followed by a 50:50 contrast + saline mixture for 6 sec, followed by a 10–15 sec saline flush. Exact values of injection parameters were dependent on patient body mass index (BMI). Per standard clinical protocol, oral and intravenous metoprolol (dose 25–100 mg oral, 5 mg intravenous) and nitroglycerin 0.4 mg sublingual were administered to all patients prior to the scans to control heart rate. Chosen tube energy was also based on patient BMI: 80 kVp for BMI < 30, 100 kVp for 30 < BMI < 40, and 120 kVp for BMI > 40. Imaging was triggered using SmartPrep software (version: Revolution CT 1.0; GE Healthcare) to obtain data at peak contrast concentration in the coronary arteries.

TABLE S1

Clinical Indications of the Patient Dataset

Clinical Indication	Number of Studies
Suspected coronary artery disease (CAD)	53
Preprocedure assessment of pulmonary vein isolation (PVI)	33
Preprocedure assessment of transcatheter aortic valve replacement (TAVR)	5
Preprocedure assessment of left ventricular assist device placement (LVAD)	9

TABLE S2

Number of Segments Given Each Score by Three Experts

Expert	Normal (Score = 0)	Hypokinetic (Score = 1)	Akinetic (Score = 2)	Dyskinetic (Score = 3)
a	1197	327	76	0
b	1038	448	106	8
c	1223	255	116	6

TABLE S3

Detailed Score List

The Scores of an Individual Segment Made by Three Experts				Number of Segments
Number of Experts with Score 0	Number of Experts with Score 1	Number of Experts with Score 2	Number of Experts with Score 3	
3	0	0	0	1022
0	3	0	0	163
2	1	0	0	145
1	2	0	0	92
0	2	1	0	79
0	0	3	0	41
0	1	2	0	37
1	1	1	0	7
0	0	2	1	5
0	1	1	1	4
0	2	0	1	3
2	0	0	1	1
1	0	1	1	1
2	0	1	0	0
1	0	2	0	0
0	0	0	3	0
1	0	0	2	0
0	1	0	2	0
0	0	1	2	0

Note.—This table shows a detailed score list. Four classes of scores, from 0 to 3, correspond to normal, hypokinetic, akinetic, and dyskinetic wall motion. Scores were made independently by three experts. To understand each row, the first row, for example, shows there are 1022 segments for which all three experts scored 0, whereas the third row shows there are 145 segments for which two of the three experts scored 0 and one of the three experts scored 1.

TABLE S4A

Kappa Analyses (Interreader Agreement)

	Interreader Agreement			
	Interreader (Binary)		Interreader (All Classes)	
Segment	Kappa	95% CI	Kappa	95% CI
Basal				
Anterior	0.63	[0.49, 0.77]	0.08	-0.24, 0.41
Anteroseptal	0.81	[0.71, 0.90]	0.50	0.22, 0.77
Inferoseptal	0.80	[0.70, 0.90]	0.41	0.05, 0.76
Inferior	0.71	[0.59, 0.85]	0.47	0.07, 0.86
Inferolateral	0.72	[0.60, 0.85]	0.56	0.01, 0.90

Anterolateral	0.71	[0.58, 0.85]	0.30	-0.04, 0.63
Mid				
Anterior	0.74	[0.62, 0.86]	0.37	0.07, 0.67
Anteroseptal	0.75	[0.64, 0.86]	0.43	0.20, 0.67
Inferoseptal	0.80	[0.69, 0.90]	0.20	-0.09, 0.48
Inferior	0.65	[0.53, 0.78]	0.55	0.27, 0.81
Inferolateral	0.72	[0.60, 0.84]	−0.01	-0.11, 0.08
Anterolateral	0.72	[0.60, 0.84]	−0.08	-0.13,-0.01
Apex				
Anterior	0.75	[0.64, 0.87]	0.40	0.16, 0.64
Septal	0.78	[0.68, 0.88]	0.24	0.01, 0.47
Inferior	0.75	[0.64, 0.86]	0.45	0.16, 0.74
Lateral	0.81	[0.71, 0.91]	0.14	-0.14, 0.43
Median	0.75		0.39	
IQR	0.72, 0.79		0.19, 0.46	

Note.—"Binary" is the segmental wall motion classification binarized into normal versus abnormal. "All classes" is the abnormal segment subclassification into hypokinetic, akinetic, or dyskinetic.

TABLE S4B

Kappa Analyses (Intermethod Agreement)

Segment	Intermethod (Training)			Intermethod (Testing)		
	RS_{CT} vs Expert A	RS_{CT} vs Expert B	RS_{CT} vs Expert C	RS_{CT} vs Expert A	RS_{CT} vs Expert B	RS_{CT} vs Expert C
	Kappa	Kappa	Kappa	Kappa	Kappa	Kappa
Basal						
Anterior	0.78	0.71	0.71	0.89	0.71	0.60
Anteroseptal	0.70	0.88	0.61	0.80	0.80	0.63
Inferoseptal	0.86	0.96	0.77	0.74	0.83	0.55
Inferior	0.89	0.75	0.82	0.81	0.70	0.46
Inferolateral	0.83	0.75	0.88	0.85	0.63	0.81
Anterolateral	0.68	0.84	0.88	0.82	0.79	0.60
Mid						
Anterior	0.94	0.63	1.00	0.73	0.67	0.77
Anteroseptal	0.82	0.75	0.91	0.86	0.78	0.81
Inferoseptal	0.85	0.82	0.90	0.69	0.66	0.80
Inferior	0.90	0.60	0.84	0.94	0.60	0.75
Inferolateral	0.91	0.69	0.73	0.81	0.60	0.88
Anterolateral	0.80	0.86	0.70	1.00	0.68	0.88
Apex						
Anterior	0.94	0.64	0.95	0.91	0.69	0.80
Septal	0.85	0.66	0.86	0.69	0.60	0.66
Inferior	0.66	0.75	0.91	0.78	0.65	0.73
Lateral	0.85	0.82	0.95	0.90	0.81	0.80
Median	0.85	0.75	0.87	0.82	0.69	0.76
IQR	0.80, 0.89	0.69, 0.83	0.76, 0.91	0.77, 0.89	0.65, 0.78	0.62, 0.80

Note.—Median and IQR were calculated across all 16 American Heart Association (AHA) segments. RS_{CT} = regional shortening from CT

TABLE S5

Performance of $RS_{CT,AHA}$* in the Validation Group

Segments	$RS_{CT,AHA}$*	Intramethod Interreader Agreement	Intermethod Agreement	Individual Equivalence Index (%)	95% CI	Individual Equivalence Index by RS_{CT} (%)	Delta
Basal							
Anterior	−0.16	130/150 (86.7)	137/150 (91.3)	−4.67	-4.68, -4.58	−4.00	−0.67
Anteroseptal	−0.16	138/150 (92.0)	143/150 (95.3)	−3.33	-3.40, -3.31	4.67	−8.00
Inferoseptal	−0.19	136/150 (90.7)	130/150 (86.7)	4.00	3.89, 4.15	4.00	0.00
Inferior	−0.17	136/150 (90.7)	137/150 (91.3)	−0.67	-0.79, -0.58	0.67	−1.34
Inferolateral	−0.20	134/150 (89.3)	140/150 (93.3)	−4.00	-4.03, -3.93	−4.00	0.00
Anterolateral	−0.16	134/150 (89.3)	140/150 (93.3)	−4.00	-4.04, -3.94	−2.00	−2.00
Mid							
Anterior	−0.20	136/150 (90.7)	140/150 (93.3)	−2.67	-2.65, -2.57	1.33	−4.00
Anteroseptal	−0.20	134/150 (89.3)	138/150 (92.0)	−2.67	-2.72, -2.55	−2.67	0.00
Inferoseptal	−0.18	138/150 (92.0)	139/150 (92.7)	−0.67	-0.75, -0.61	3.33	−4.00
Inferior	−0.18	126/150 (84.0)	136/150 (90.7)	−6.67	-6.71, -6.60	−6.67	0.00
Inferolateral	−0.21	136/150 (90.7)	136/150 (90.7)	0.00	-0.06, 0.14	−0.67	0.67
Anterolateral	−0.17	132/150 (88.0)	141/150 (94.0)	−6.00	-6.03, -5.92	−6.00	0.00
Apical							
Anterior	−0.23	136/150 (90.7)	138/150 (92.0)	−1.33	-1.35, -1.19	−0.67	−0.66
Septal	−0.21	134/150 (89.3)	136/150 (90.7)	−1.33	-1.36, -1.21	4.00	−5.33
Inferior	−0.22	140/150 (93.3)	139/150 (92.7)	0.67	0.62, 0.76	4.00	−3.33
Lateral	−0.19	138/150 (92.0)	140/150 (93.3)	−1.33	-1.37, -1.22	−1.33	0.00
All Segments		2158/2400 (89.9)	2210/2400 (92.1)	−2.17	-2.18, -2.14	−0.38	−1.79

Note.—This table shows the specific threshold $RS_{CT,AHA}$* for each American Heart Association (AHA) segment (the second column), the corresponding intermethod agreement rate (the fourth column), and the corresponding individual equivalence index and its 95% CI (the fifth and sixth columns). We also compared the individual equivalence index by $RS_{CT,AHA}$* (the fifth column) with that by single-threshold RS_{CT}* (the seventh column) and calculated the delta (the last column) = the fifth column minus the sixth column. The last row shows the cumulative performance for all segments. Percentages are in parentheses. $RS_{CT,AHA}$* = the optimal threshold of RS_{CT} for each AHA segment that led to the minimum value of γ.

TABLE S6

Performance of RS_{CT} Across Clinical Indications

Clinical indication	Intramethod Interreader Agreement	Intermethod Agreement	Individual Equivalence Index (%)	95% CI
CAD	2318/2544 (91.17)	2347/2544 (92.25)	−1.14	-1.13,-1.09
PVI	1424/1584 (89.90)	1454/1584 (91.79)	−1.89	-1.94,-1.88
VAD	374/432 (86.6)	371/432 (85.9)	0.69	0.62, 0.76
TAVR	192/240 (80.0)	207/240 (86.3)	−6.25	-6.35, -6.23

Note.—Both training and validation groups were used here. CAD = coronary artery disease, PVI = pulmonary vein isolation, RS_{CT} = regional shortening from CT, TAVR = transcatheter aortic valve replacement, VAD = ventricular assist device. Percentages are in parentheses.

End-Diastole:

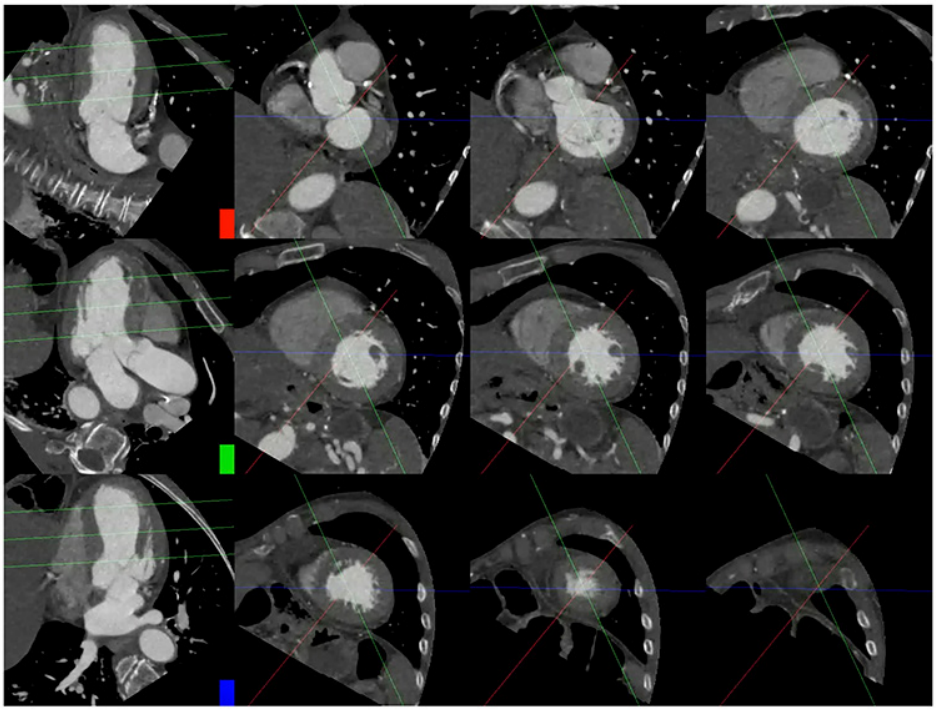

End-systole:

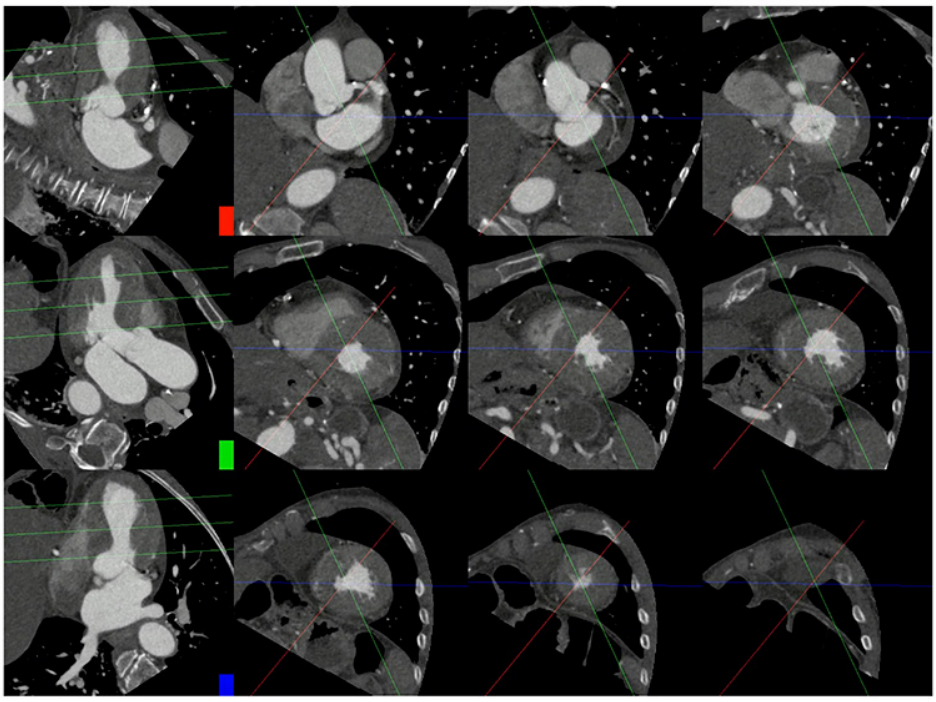

Figure S1: Top and bottom figures are screenshots of the end-diastole frame and the end-systole frame of a cine movie of the cardiac function shown to the experts for visual labeling. The movie contains three long-axis (LAX) planes in the first column and nine short-axis (SAX) planes from the basal to apex of the left ventricle (LV) in the right three columns. The two-chamber view, three-chamber view, and four-chamber view are represented by red, green, and blue lines in the SAX plane image. The third, fifth, and seventh SAX planes are represented by the green lines in the LAX planes.

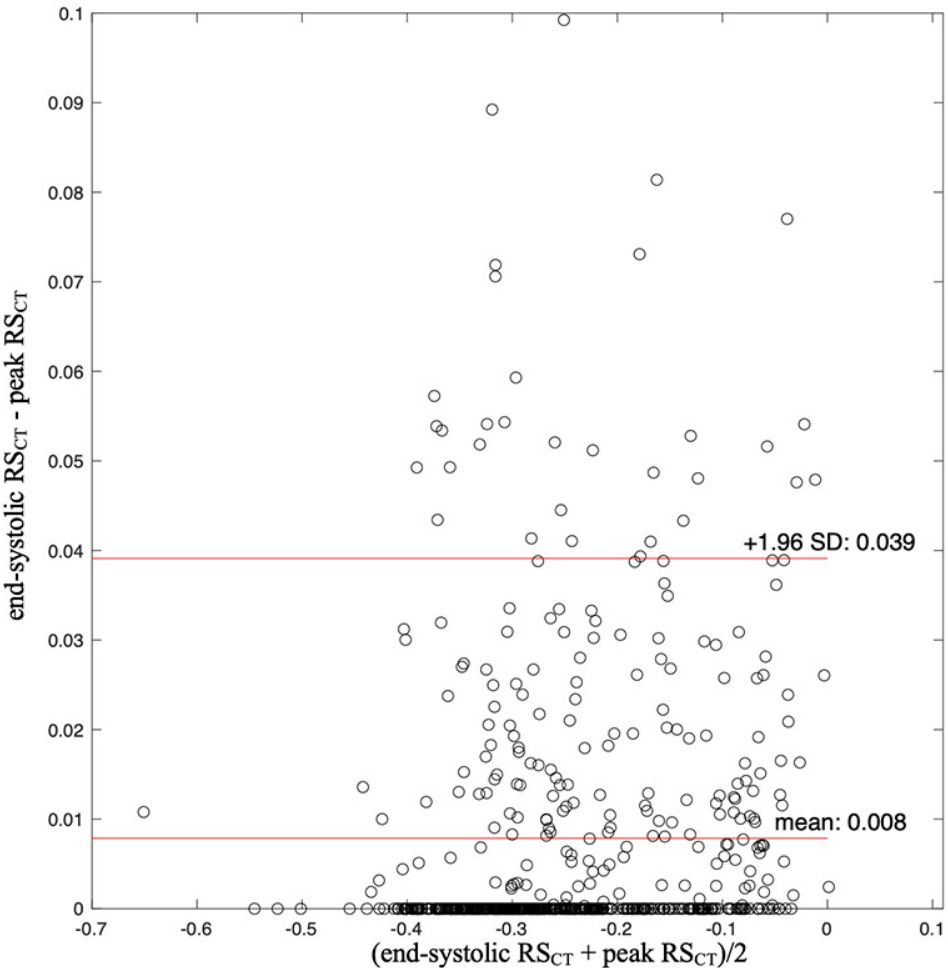

Figure S2: The Bland-Altman plot for peak RS_{CT} and end-systolic RS_{CT} measured in 6 basal segments from our 100-patient group. The y-axis lower limit is 0 because end-systolic RS_{CT}–peak RSCT is always above or equal to 0; 379 of 600 points had a y-coordinate (difference) as 0. RS_{CT} = regional shortening from CT.

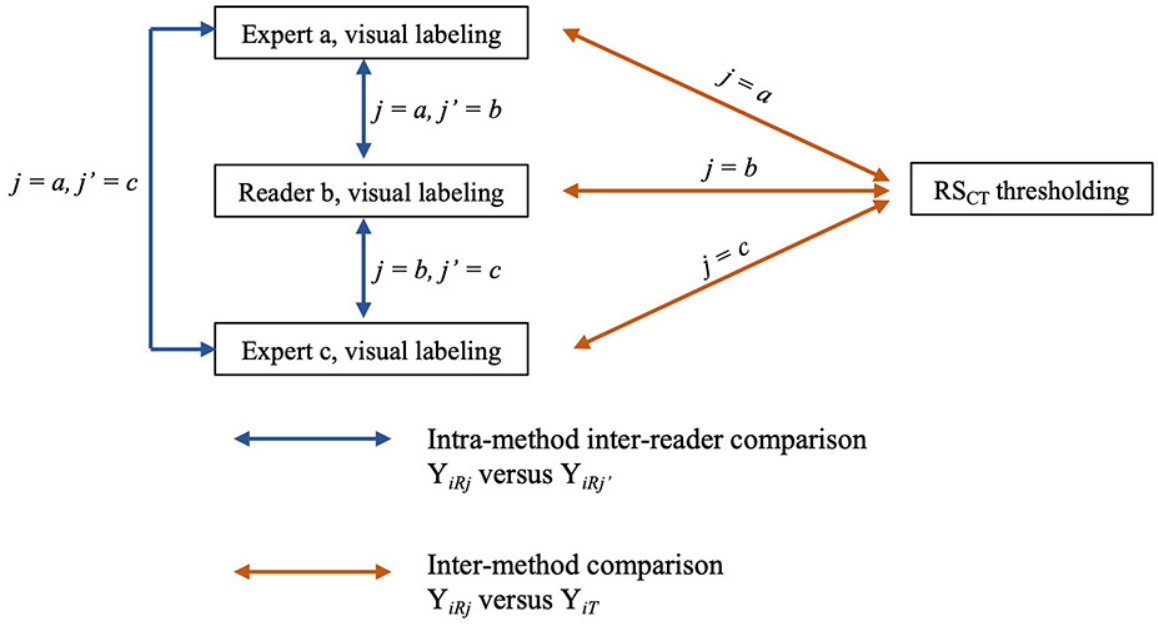

Figure S3: This figure shows the three groups of intramethod interreader comparisons (blue arrows, the first term in the Equation 3) and the three groups of intermethod comparisons (orange arrows, the second term in the Equation 3). The individual equivalence index is equal to the accumulative agreement rate for three interreader comparisons minus the accumulative agreement rate for the three intermethod comparisons. The definitions of Y_{iRj}, $Y_{iRj'}$, and Y_{iT} can be found in the Interchangeability Analysis section.